Preparation of Ni(OH)₂/MWCNTs Composite for Supercapacitor Application

Junhua Wu[1,], Fei Ge[1] and Yingjie Li[2]*

[1] School of Automotive and Traffic Engineering, Nanjing Forestry University, Nanjing 210037, China
[2] College of Chemistry and Chemical Engineering, Shanghai University of Engineering Science，Shanghai 201620,China
[*]E-mail: wujunhuanj@163.com

In this work, flexible supercapacitor electrodes were fabricated using a simple chemical strategy in which nanocrystalline $Ni(OH)_2$ was coated on multiwalled carbon nanotubes (MWCNTs). $Ni(OH)_2$/MWCNT thin films were deposited on large-area flexible substrates using the simple successive ionic layer adsorption and reaction (SILAR) strategy proposed in this report. The specific capacitance (SC) of the $Ni(OH)_2$/MWCNT films was determined to be 1466 F/g in aqueous KOH solution (2 M) at a scan rate of 5 mV/s. A facile three-beaker SILAR configuration was used to prepare the electrodes at room temperature, providing a facile route to the fabrication of flexible supercapacitors with high energy and power levels. An extensive variety of $Ni(OH)_2$/MWCNT-like materials could be prepared using a general strategy based on our proposed technique, and these materials could be used in applications beyond electrochemical energy storage.

Keywords: Supercapacitor; $Ni(OH)_2$; Graphene; Vehicular application; Multi-walled carbon nanotube

1. INTRODUCTION

The continuing increase in car ownership and vehicle utility have led to a rise in greenhouse gas emissions and energy use. The global transport energy demand showed an average annual increase of 1.6% (2007 – 2030), as determined by the International Energy Agency (IEA, 2009b). Therefore, a substantial portion of the required energy for automobiles has shifted from petroleum to other energy sources. To cater to the ecological and societal need for clean transportation, greener propulsion solutions are of interest to many original automotive equipment manufacturers. Both automotive enterprises and governments have agreed on the proposal of new energy vehicles (NEV), which

evolved into a "three horizontal and three vertical" technique route pattern. The "three horizontal" portion represents a multi-energy driving force for the motor, control system, and power management system, while the "three vertical" portion represents hybrid electric vehicles (HEV), pure electric vehicles (PEV), and fuel cell vehicles (FCV). Among these systems, electrical energy storage technology, mainly as it relates to NEV-type technology, has the potential for further studies and breakthroughs. As an electrochemical capacitor and the most ordinary electrical energy storage technology applied to vehicles, supercapacitors have high potential to be used in the energy field due to their environmental friendliness, prolonged cycle life and high power density. Furthermore, the energy and power gaps between conventional physical capacitors and secondary batteries/fuel cells could be bridged by supercapacitors. Hence, supercapacitors have gained extensive use in the fields of advanced energy storage apparatuses and electric vehicles.

According to the energy storage mechanism, there are two types of supercapacitors: electrical double-layer capacitors (EDLCs) and pseudocapacitors. The former store energy on the electrode surface via fast charge adsorption/desorption [1, 2], while the latter store energy through surface Faradaic reactions between the electrolyte ions and electrode materials [3, 4]. Carbon materials, including activated carbon [5, 6], carbon nanotubes [7] and graphene [8, 9], have been extensively used in EDLC electrodes. Promising pseudocapacitive materials include transition metal oxides [10-12], hydroxides [13, 14] and conductive polymers [15, 16].

The SCs of carbon materials are ordinarily below 200 F/g, due to their undesirable energy storage mechanism and specific surface area. However, significantly larger SCs are obtained due to the fast Faradaic reactions of transition metal oxides and hydroxides [17-25]. With respect to the preparation of supercapacitors, nickel hydroxides are attractive materials due to their long cycle behavior and high SCs [26]. Sun and co-workers [20] reported an SC of 1568 F/g when a mechanically assisted solid-state reaction technique was used for the preparation of a $Ni(OH)_2$/graphene hybrid. Yan and co-workers [26] reported an SC of 816 F/g when a microwave heating route was used for the synthesis of a $Ni(OH)_2$/graphene hybrid. Chen and co-workers [27] proposed the formation of a $Ni(OH)_2$/graphene composite with long cycle life and high rate behavior through the preparation of $Ni(OH)_2$ nanoparticles confined in graphene films. The primary factors contributing to the high performance of the abovementioned $Ni(OH)_2$/graphene hybrids are the desirable conductivity of graphene for electronic and ionic transport and the high capacitance of $Ni(OH)_2$. Nevertheless, the above hybrids exhibit limited SCs resulting from the lower SCs of carbon materials due to the hydroxide ratios in the total mass of the hybrid.

In this work, a $Ni(OH)_2$/MWCNT composite was prepared directly on flexible substrates to be compatible with supercapacitors using our proposed facile and cost-effective commercial synthesis technique. Furthermore, the composition and surface area of the successive ionic layer adsorption and reaction (SILAR)-grown films were measured through corresponding characterization techniques. A range of measurements, including impedance, charge/discharge, and cyclic voltammograms (CVs), were used to investigate the electrochemical features of the $Ni(OH)_2$/MWCNT films. Due to the connection between the electrically conductive MWCNTs and the pseudocapacitive sponge-like $Ni(OH)_2$ nanoparticles, the SC of the $Ni(OH)_2$/MWCNT sample was high, as shown in the CVs.

2. EXPERIMENTS

The substrate was successively immersed in separate anionic and cationic precursor solutions at ambient temperature, where a sequential reaction occurred on the surface of the electrode. Through this reaction, the $Ni(OH)_2$/MWCNT thin film was synthesized using the facile SILAR strategy. With respect to the SILAR strategy, the $Ni(OH)_2$/MWCNT thin film was deposited directly on the stainless-steel substrate in the three-beaker SILAR configuration. In brief, stable dispersions were formed by sonication of the functionalized MWCNTs (0.01 g) in Milli-Q water (50 mL, 18 MΩ·cm) for a few hours. The functionalization of the MWCNTs was briefly examined after collecting the above dispersed MWCNTs into the first beaker. As a source of Ni^{2+} ions, 0.1 M of aqueous nickel sulfate solution was introduced into the second beaker, and an aqueous ammonia solution was introduced to adjust the pH to approximately 12. Eventually, deionized water was introduced to the last beaker, along with several drops of 6% H_2O_2 solution, which acted as the source of hydroxyl ions, and the solution was maintained at 343 K. The procedure began by dipping the stainless-steel substrates pre-treated by ultrasound and cleaning into the aforementioned MWCNT solution for 20 s, and the MWCNTs were adsorbed onto the substrate surface. The adsorption of nickel complex ions to the pre-adsorbed MWCNT surface was achieved after dipping this substrate into an alkaline nickel sulfate solution for 10 s. $Ni(OH)_2$ nanoparticles were produced through a reaction on the surfaces of the as-prepared MWCNTs after this substrate was immersed in the H_2O_2 solution and maintained at 343 K for 10 s. To make the $Ni(OH)_2$/MWCNT thin film thicker, we ran the same cycle several times.

A Cu Kα (λ = 1.5418 Å) source was applied to a Rigaku Rotalflex RU-200B diffractometer equipped with a Ni filter and used for a crystallographic investigation at 40 kV and 40 mA with a scan rate of 0.02 s^{-1}. A VG Multilab 2000 obtained from Thermo VG Scientific U.K. was used for X-ray photoelectron spectroscopy (XPS); XPS is also referred to the Electron Spectroscopy for Chemical Analyzer or ESCA. An ASAP-2010 surface area analyzer was used for Brunauer–Emmett–Teller (BET) analysis to determine the adsorption/desorption of N_2. An electrochemical cell involved AMETEK Solartron analytical system model 1400 was used for CV. With respect to this cell, the working, counter and reference electrodes were $Ni(OH)_2$, platinum and Ag/AgCl, respectively. Galvanostatic charge/discharge analysis was performed using an 8-channel advanced battery cycler (WonATech-WBCS-3000 model). A multi-impedance test configuration was used for the electrochemical impedance spectroscopy analysis, in which the AC amplitude was 10 mV and the frequency ranged from 10 kHz to 10 mHz.

3. RESULTS AND DISCUSSION

The flexible stainless-steel (FSS) substrates were successively immersed in separate anionic and cationic precursor solutions to yield $Ni(OH)_2$/MWCNT thin films. An ultrasonicator was used to disperse the functionalized MWCNTs into deionized water. MWCNTs were adsorbed on the substrate via attractive forces (van der Waals, cohesive, and other chemical attractive forces) between the MWCNTs and substrate during the immersion of the FSS substrate into the above solution. With

respect to the second beaker, NH_4OH (25% extra pure) and aqueous ammonia solution was mixed with a source of nickel, $NiSO_4$ (0.1 M), and continually stirred to obtain an alkaline condition. According to the growth kinetics, the film grows via ion-by-ion deposition at nucleation sites on the immersed surface [28-30]. During the initial stage, the $Ni(OH)_2$ ion product was more prevalent than the solubility product, with the addition of the aqueous ammonia solution into the nickel sulfate solution. In addition, a turbid solution was obtained due to $Ni(OH)_2$ precipitation based on the following equation:

$$NiSO_4 + 2NH_4OH \rightarrow Ni(OH)_2 + 2NH_4^+ + SO_4^-$$

Nevertheless, as surplus ammonia solution was further added, the complex ion of $Ni(NH_3)_n^{2+}$ ($n = 1–4$) was produced, with n = 4 being the most stable coordination number [31], thus leading to the reduction in the concentration of Ni^{2+} ions. A transparent and clear solution was obtained due to this sophisticated formation, as shown in the following equation:

$$Ni(OH)_2 + 4NH_4^+ \rightarrow Ni(NH_3)_4^{2+} + 2H_2O + 2H^+$$
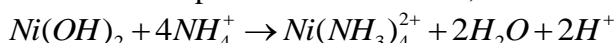
Due to the electrostatic force of attraction between the functionalized MWCNTs and the $Ni(NH_3)_4^{2+}$ ions, the $Ni(NH_3)_4^{2+}$ ions present in the solution preferentially adsorbed onto the MWCNT walls occurred during the immersion of the substrate into the aforementioned solution.

It is worth noting that a source of OH^- ions appeared due to the addition of several drops of H_2O_2 into the deionized water after heat treatment at around the boiling point. As a catalyst in this test, H_2O_2 reduced the activation energy of the chemical reaction, providing an alternative way for the reaction to proceed. Then, the wet substrate was immersed in deionized water at 343 K. An adherent $Ni(OH)_2$ layer (only several nanometers thick) was deposited as follows:

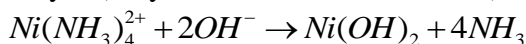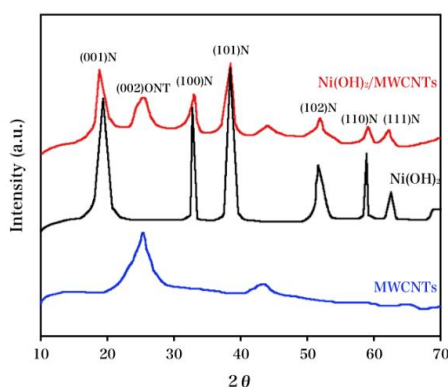$$Ni(NH_3)_4^{2+} + 2OH^- \rightarrow Ni(OH)_2 + 4NH_3$$

Fig. 1 shows the XRD profiles of the $Ni(OH)_2$, MWCNT and $Ni(OH)_2$/MWCNT powders. It can be clearly seen that the MWCNT and $Ni(OH)_2$/MWCNT powders both exhibited the characteristic graphitic (002) peak of MWCNTs at 25.55° [32].

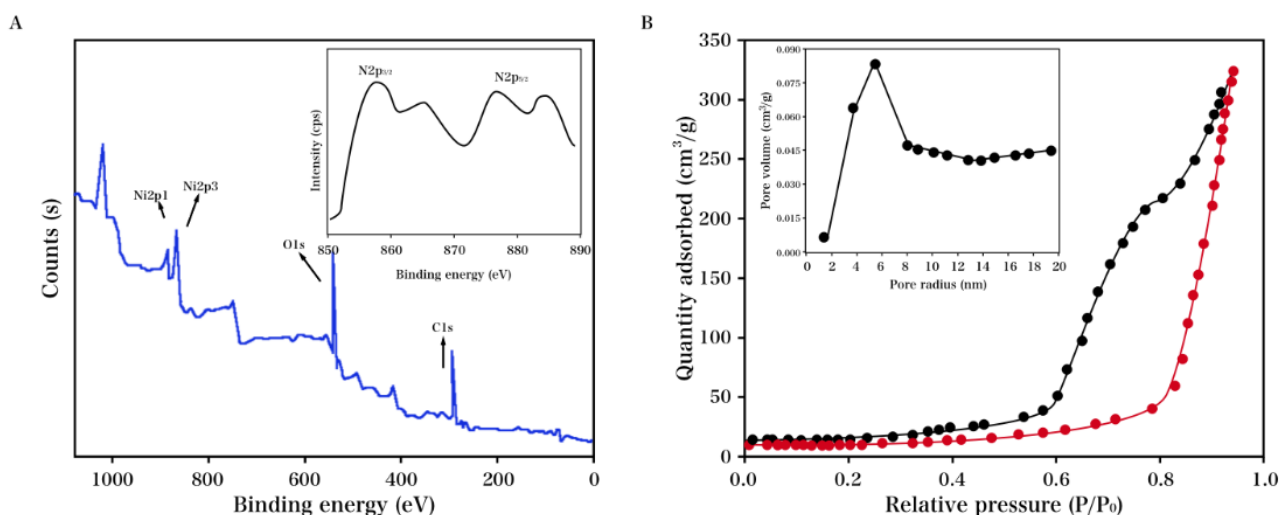**Figure 1.** XRD profiles of the $Ni(OH)_2$, MWCNT, and $Ni(OH)_2$/MWCNT powders.

β-phase nickel hydroxide with a hexagonal brucite structure was found, corresponding to the reflections along the (100), (002), (100), (101), (102), (110), and (111) planes [32], which is consistent

with the standard pattern (JCPDS 01-1047). In addition, broad diffraction peaks were observed, suggesting the nanocrystalline property of pure $Ni(OH)_2$ and $Ni(OH)_2$ coated on the MWCNTs. This phase is beneficial for supercapacitors because it creates a path for penetration through the bulk of the $Ni(OH)_2$ material, and the entire electrode material can be used for energy storage [33, 34].

We also carried out XPS measurements to further understand the composition of the terminal products. The $Ni(OH)_2$/MWCNT composite was characterized by an XPS general survey spectrum, as shown in Fig. 2A. O1s and Ni2p peaks were observed, confirming that the CNTs were oxidized and $Ni(OH)_2$ was decorated on the CNT walls. The binding energy of $Ni2p_{3/2}$ was approximately 855.7 eV, which is consistent with the previously reported value [35]. As indicated in the inset of Fig. 2A, the Ni2p core level was characterized by a higher resolution XPS spectrum (850 – 870 eV). Two spin–orbit doublets typical of Ni^{3+} and Ni^{2+} and two shakeup satellites were recorded in this spectrum.

The $Ni(OH)_2$/MWCNT composite was characterized by its nitrogen adsorption–desorption isotherm profile, and the inset shows the corresponding pore size distribution (Fig. 2B). The nitrogen isotherm was a type IV isotherm, and there was a small hysteresis loop. When the relative pressure (p/p_0) range was 0.4 to 0.6, a small step of nitrogen adsorption and desorption branching was observed, suggesting that mesopores were present. The $Ni(OH)_2$/MWCNT composite was measured to have a BET surface area of 157 m^2/g, according to the nitrogen adsorption–desorption isotherm. It can be seen that the mesopore distribution was centered at 4.11 nm and exhibited a narrow pore size distribution, as indicated by the pore size distribution data obtained via the BJH (Barrett–Joyner–Halenda) technique from the adsorption branches of the nitrogen isotherms. These mesoporous networks of sponge-like nanoparticles provide low-resistance pathways through the porous structure, which helps improve the charge transport and power capability [36].
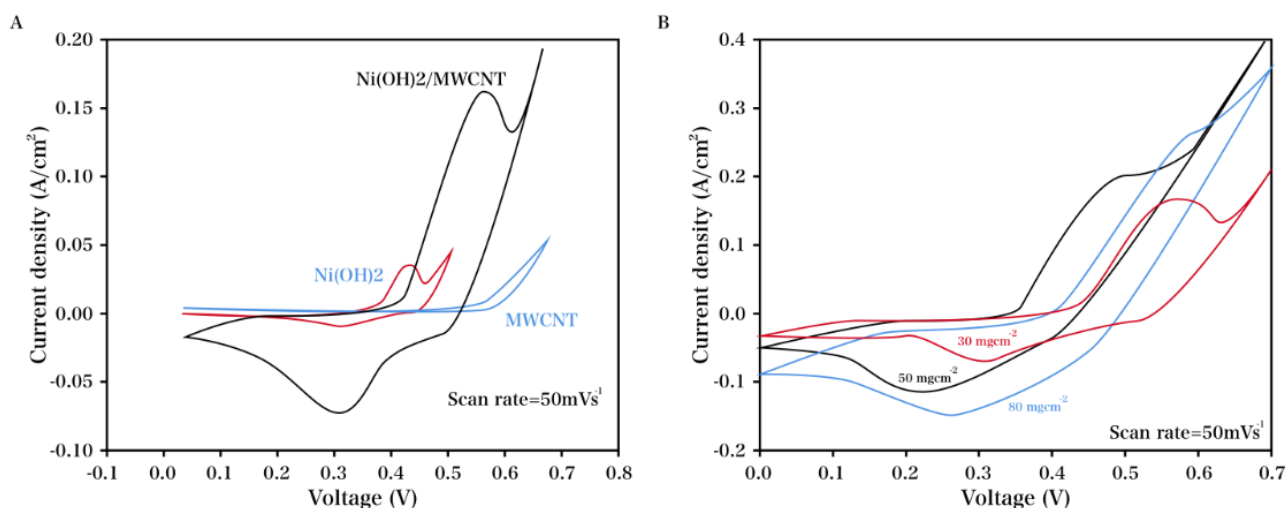

Figure 2. (A) XPS profiles of the $Ni(OH)_2$/MWCNT composite. Inset: XPS profile for the Ni_{2p} core level. (B) Nitrogen adsorption–desorption isotherms of the $Ni(OH)_2$/MWCNT composite.

As indicated in Fig. 3A, the MWCNTs, $Ni(OH)_2$, and $Ni(OH)_2$/MWCNT composite were characterized via CV in KOH electrolyte (2 M) at a scan rate of 50 mV/s. The difference between the

electric double layer capacitance and capacitance characteristics can be determined by the CV shape, which ordinarily approaches an ideal rectangular shape. The primary contributing factor of the capacity was a pseudocapacitance, as indicated by the redox peaks for the $Ni(OH)_2$/MWCNT and $Ni(OH)_2$ specimens.

We fully utilized the advantages of the ionic layer adsorption and reaction process to enable precise capacity control of the electrodes by controlling the thickness of the $Ni(OH)_2$/MWCNT films [37]. The $Ni(OH)_2$/MWCNT electrodes (30 to 80 mg/cm^2) were characterized via mass-dependent CV at a scan rate of 50 mV/s (Fig. 3B). As the film thickness increased, an increase in the voltammetric current of the $Ni(OH)_2$/MWCNT electrode was observed, suggesting that the in-film thickness increase led to the SC reduction. With respect to a mass loading (ML) of 30 mg/cm^2, 1144 F/g was calculated as the maximal value (scan rate: 50 mV/s). As the ML increased in the range of 30 to 80 mg/cm^2, a sharp decrease in the SC was recorded in a range of 1141 to 444 F/g.


Figure 3. (A) CV profiles of MWCNTs, $Ni(OH)_2$, and the $Ni(OH)_2$/MWCNT composite and (B) mass-dependent CV of the $Ni(OH)_2$/MWCNT electrodes in KOH electrolyte (2 M) at a scan rate of 50 mV/s.
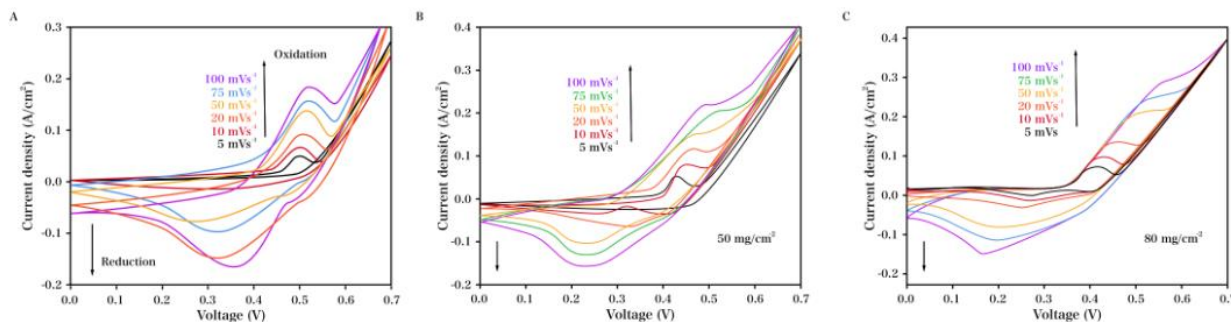
Figure 4. CV profiles of the $Ni(OH)_2$/MWCNT hybrids at scan rates of (A) 30 mg/cm^2, (B) 50 mg/cm^2 and (C) 80 mg/cm^2.

Ni(OH)$_2$/MWCNT hybrids with varying thicknesses were characterized via CV at varying scan rates, as indicated in Fig. 4A–C. A slow increase in the current for the CV measurement with increasing scan rate was observed, indicating the direct proportional relationship between the voltammetric current and the scan rate, further suggesting a desirable capacitive performance. The SC exhibited maximal values of 772, 1007, and 1466 F/g when the MLs were 80, 50 and 30 mg/cm^2, respectively (scan rate: 5 mV/s). The SC was maintained at 995 F/g (ML: 30 mg/cm^2) when the scan rate was as high as 100 mV/s. Furthermore, a high surface area and a short diffusion path for ion exchange were achieved by the thin Ni(OH)$_2$ layer. In addition, compared with Ni(OH)$_2$, the core MWCNTs exhibited higher electrical conductivity, providing a fast path for charge transfer. An increase in the solution infiltration rate, along with the facilitation of ion insertion/extraction and electron transport in the electrode were achieved due to the porous network structure, the high surface area, and the synergetic effects of the MWCNTs and Ni(OH)$_2$ [38-40]. The cycling life test for the Ni(OH)$_2$/MWCNT electrode for different mass loadings was performed at a scan rate of 100 mV/s over 1000 cycles. It can be seen that all the CV curves overlapped, which indicates good cycling stability.
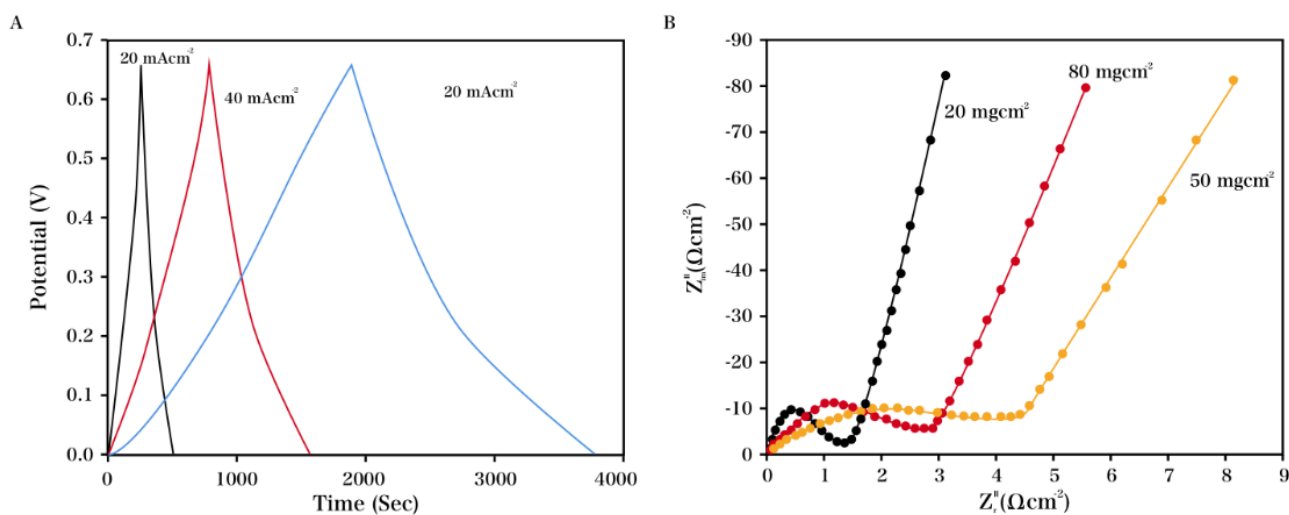
Figure 5. (A) Constant current charge/discharge profiles of varying densities of the Ni(OH)$_2$/MWCNT thin films with an ML of 30 mg/cm^2 and (B) impedance spectra of the Ni(OH)$_2$/MWCNT thin films with varying MLs (10^3 to 10^{-3} Hz), where the inset shows the equivalent circuit for the Ni(OH)$_2$/MWCNT composite.

The Ni(OH)$_2$/MWCNT thin films with varying densities (ML: 30 mg cm^{-2}) were characterized by their constant current charge/discharge profiles (Fig. 5A). Symmetry was observed between the charging profiles and the corresponding discharging patterns. A low voltage loss was observed, suggesting a low internal resistance. The Ni(OH)$_2$/MWCNT composite was electrochemically reversible with an SC as large as 1522 F/g. In addition, the charge/discharge and CV measurements showed comparable SC values. As shown in the impedance plots (Fig. 5B), an almost straight line along the imaginary axis was observed at low frequencies, and a partial semicircle was observed at high frequencies, due to the mass transport limit and Faradaic charge transfer resistance, respectively.

The charge-transfer resistance (Rct) over the interface between the electrolyte and Ni(OH)$_2$/MWCNT electrode was calculated based on the diameter, while the solution resistance (Rsol) was obtained by the high-frequency intercept of the semicircle on the real axis [41]. These values are superior to those of similar, previously reported symmetrical systems. Table 1 shows a comparison of the maximum energy density of our proposed material with other materials in the literature.

Table 1. Maximum energy density comparison of our proposed Ni(OH)$_2$/MWCNT composite with materials from other reports.

Material	Maximum energy density (Wh/kg)	Reference
Prussian Blue modified positive electrode	7.68	[42]
Activated-N-doped graphene	66	[43]
GO/PPy	15	[44]
Papers coated with carbon nanotubes	41	[45]
Ni(OH)$_2$/Graphene	77.8	[26]
Ni(OH)$_2$/MWCNT	17.9	This work

4. CONCLUSIONS

This work proposed the decoration of nanocrystalline Ni(OH)$_2$ on MWCNTs using a facile chemical technique involving a bottom-up strategy. The layer-by-layer assembly was alternated, leading to the formation of a porous MWCNT network as well as fast electronic and ion conducting channels in the presence of an electrolyte. Additionally, high capacitance was achieved after Ni(OH)$_2$ was conformally coated onto the MWCNTs. Therefore, high-performance electrodes could be designed and used for supercapacitor applications based on the above systems.

References

1. D. Pech, M. Brunet, H. Durou, P. Huang, V. Mochalin, Y. Gogotsi, P. Taberna and P. Simon, *Nature Nanotechnology*, 5 (2010) 651.
2. Y. Wang, Z. Shi, Y. Huang, Y. Ma, C. Wang, M. Chen and Y. Chen, *J Phys Chem C*, 113 (2009) 13103.
3. M. Vidotti, M. Silva, R. Salvador, S.C. de Torresi and L. Dall'Antonia, *Electrochimica Acta*, 53 (2008) 4030.
4. C. Yang and P. Liu, *Synthetic Metals*, 160 (2010) 768.
5. L. Demarconnay, E. Raymundo-Piñero and F. Béguin, *Electrochemistry Communications*, 12 (2010) 1275.
6. C. Qin, L. Xing, G. Yin, X. Bai and J. Zheng, *Transactions of Nonferrous Metals Society of China*, 19 (2009) s738.
7. A. Izadi-Najafabadi, T. Yamada, D.N. Futaba, M. Yudasaka, H. Takagi, H. Hatori, S. Iijima and K. Hata, *ACS Nano*, 5 (2011) 811.

8.　C. Liu, Z. Yu, D. Neff, A. Zhamu and B.Z. Jang, *Nano Letters*, 10 (2010) 4863.
9.　X. Lin, X. Shen, Q. Zheng, N. Yousefi, L. Ye, Y. Mai and J. Kim, *ACS Nano*, 6 (2012) 10708.
10. J. Huang, J. Zhu, K. Cheng, Y. Xu, D. Cao and G. Wang, *Electrochimica Acta*, 75 (2012) 273.
11. Y. Li, S. Chang, X. Liu, J. Huang, J. Yin, G. Wang and D. Cao, *Electrochimica Acta*, 85 (2012) 393.
12. S. Vijayakumar, S. Nagamuthu and G. Muralidharan, *ACS Applied Materials & Interfaces*, 5 (2013) 2188.
13. L. Kong, J. Lang, M. Liu, Y. Luo and L. Kang, *Journal of Power Sources*, 194 (2009) 1194.
14. Z. Tang, C.h. Tang and H. Gong, *Adv Funct Mater*, 22 (2012) 1272.
15. G. Snook, P. Kao and A. Best, *Journal of Power Sources*, 196 (2011) 1.
16. H. Lee, H. Kim, M.S. Cho, J. Choi and Y. Lee, *Electrochimica Acta*, 56 (2011) 7460.
17. S. Yan, H. Wang, P. Qu, Y. Zhang and Z. Xiao, *Synthetic Metals*, 159 (2009) 158.
18. Z. Wu, G. Zhou, L. Yin, W. Ren, F. Li and H. Cheng, *Nano Energy*, 1 (2012) 107.
19. C. Wu, C. Fan, I. Sun, W. Tsai and J. Chang, *Journal of Power Sources*, 196 (2011) 7828.
20. Z. Sun and X. Lu, *Ind. Eng. Chem. Res.*, 51 (2012) 9973.
21. G. Hasegawa, K. Kanamori, T. Kiyomura, H. Kurata, T. Abe and K. Nakanishi, *Chemistry of Materials*, 28 (2016) 3944.
22. X. Wang, H. Xia, X. Wang, J. Gao, B. Shi and Y. Fang, *Journal of Alloys and Compounds*, 686 (2016) 969.
23. Y. Tang, Z. Liu, W. Guo, T. Chen, Y. Qiao, S. Mu, Y. Zhao and F. Gao, *Electrochimica Acta*, 190 (2016) 118.
24. H. Wang, L. Ma, M. Gan, T. Zhou, X. Sun, W. Dai, H. Wang and S. Wang, *Composites Part B: Engineering*, 92 (2016) 405.
25. Y. Zhang, J. Wang, H. Wei, J. Hao, J. Mu, P. Cao, J. Wang and S. Zhao, *Materials Letters*, 162 (2016) 67.
26. J. Yan, Z. Fan, W. Sun, G. Ning, T. Wei, Q. Zhang, R. Zhang, L. Zhi and F. Wei, *Adv Funct Mater*, 22 (2012) 2632.
27. S. Chen, J. Zhu, L. Qiu, D. Li and X. Wang, *Chemistry–A European Journal*, 19 (2013) 7631.
28. B. Li, F. Dai, Q. Xiao, L. Yang, J. Shen, C. Zhang and M. Cai, *Energy & Environmental Science*, 9 (2016) 102.
29. A. Mohammadi, S. Peighambardoust, A. Entezami and N. Arsalani, *Journal of Materials Science: Materials in Electronics*, 28 (2017) 5776.
30. H. Naderi, P. Norouzi and M. Ganjali, *Applied Surface Science*, 366 (2016) 552.
31. F. Cao, M. Zhao, Y. Yu, B. Chen, Y. Huang, J. Yang, X. Cao, Q. Lu, X. Zhang and Z. Zhang, *Journal of the American Chemical Society*, 138 (2016) 6924.
32. D. Dubal, G. Gund, C. Lokhande and R. Holze, *ACS Applied Materials & Interfaces*, 5 (2013) 2446.
33. R. Li, S. Wang, Z. Huang, F. Lu and T. He, *Journal of Power Sources*, 312 (2016) 156.
34. Y. Yang, D. Cheng, S. Chen, Y. Guan and J. Xiong, *Electrochimica Acta*, 193 (2016) 116.
35. W. Chen, Y. Yang and H. Shao, *Journal of Power Sources*, 196 (2011) 488.
36. J. Liu, M. Zheng, X. Shi, H. Zeng and H. Xia, *Advanced Functional Materials*, 26 (2016) 919.
37. Y. Xu, L. Wang, P. Cao, C. Cai, Y. Fu and X. Ma, *Journal of Power Sources*, 306 (2016) 742.
38. H. Fan, H. Wang, N. Zhao, X. Zhang and J. Xu, *Journal of Materials Chemistry*, 22 (2012) 2774.
39. C. Ghimbeu, E. Raymundo-Piñero, P. Fioux, F. Béguin and C. Vix-Guterl, *Journal of Materials Chemistry*, 21 (2011) 13268.
40. L. Mao, K. Zhang, H.S.O. Chan and J. Wu, *Journal of Materials Chemistry*, 22 (2012) 1845.
41. M. Najafpour, M. Tabrizi and B. Haghighi, *Dalton Transactions*, 41 (2012) 3906.
42. P. Díaz, Z. González, R. Santamaría, M. Granda, R. Menéndez and C. Blanco, *Electrochimica Acta*, 212 (2016) 848.
43. Q. Fan, M. Yang, Q. Meng, B. Cao and Y. Yu, *Journal of The Electrochemical Society*, 163 (2016) A1736.

44. A. Singh and A. Chandra, *Journal of Applied Electrochemistry*, 43 (2013) 773.
45. Y. Kang, H. Chung, C.-H. Han and W. Kim, *Nanotechnology*, 23 (2012) 065401.